Ultrahigh energy gamma rays in the geomagnetic field and atmosphere

H. P. Vankov
Institute for Nuclear Research and Nuclear Energy, Sofia 1784, Bulgaria

N. Inoue
Department of Physics, Saitama University, Saitama 338-8570, Japan

K. Shinozaki
Institute for Cosmic Ray Research, University of Tokyo, Chiba 277-8582, Japan

(Received 30 October 2002; published 19 February 2003)

The nature and origin of ultrahigh energy (UHE, referring to $>10^{19}$ eV) cosmic rays are great mysteries in modern astrophysics. The current theories for their explanation include the so-called top-down decay scenarios whose main signature is a large ratio of UHE gamma rays to protons. An important step in determining the primary composition at ultrahigh energies is the study of air shower development. UHE gamma ray induced showers are affected by the Landau-Pomeranchuk-Migdal (LPM) effect and the geomagnetic cascading process. In this work extensive simulations have been carried out to study the characteristics of air showers from UHE gamma rays. At energies above several times 10^{19} eV the shower is affected by geomagnetic cascading rather than by the LPM effect. The properties of the longitudinal development such as the average depth of the shower maximum or its fluctuations depend strongly on both primary energy and incident direction. This feature may provide possible evidence of UHE gamma ray presence by fluorescence detectors.

DOI: 10.1103/PhysRevD.67.043002 PACS number(s): 96.40.Pq, 13.66.−a

I. INTRODUCTION

Ultrahigh energy (UHE; $>10^{19}$ eV) cosmic ray research was initiated about 40 years ago. Several experiments have been carried out (see [1] for a review) and at present the Akeno Giant Air Shower Array (AGASA) [2], HiRes [3], and Yakutsuk [4] experiments are in operation to observe air showers initiated by UHE cosmic rays. Today the number of recorded events is already big enough to convince even strong skeptics that the cosmic ray energy spectrum extends well beyond the theoretically expected Greisen-Zatzepin-Kuz'min (GZK) cutoff around 5×10^{19} eV [5]. The origin and nature of these particles are still unsolved questions. The problem is that it is very difficult to extend our understanding of particle acceleration to such extraordinarily high energies, and the propagation of these particles in the cosmic microwave background (CMB) radiation restricts the distance to their potential sources within several tens of megaparsecs ($1\ \mathrm{Mpc}=3.1\times10^{24}$ cm).

Various models of UHE cosmic ray origin have been proposed. They are currently a subject of very intensive discussion (see [6] for a review). Models can be categorized into two basic groups of ''scenarios'': ''bottom up'' and ''top down.''

Conventional bottom-up scenarios look for astrophysical sources called ''zevatrons'' ($1\ \mathrm{ZeV}=10^{21}$ eV) that can accelerate particles to energies in excess of 10^{20} eV. The composition of UHE cosmic rays is expected to be hadronic. Possible candidates include clusters of galaxies, active galactic nuclei (AGN) radio lobes, AGN central regions, young neutron stars, magnetars, gamma ray bursts, etc.

In the top-down scenarios UHE cosmic rays instead of being accelerated are generated from decay of some exotic very heavy (10^{22}–10^{25} eV)X particles that are supposed to have been formed in the early universe. The sources of X particles may be topological defects (cosmic strings, cosmic necklaces, magnetic monopoles, domain walls) [7] or long-lived superheavy relic particles [8].

The cascade process initiated by a superhigh energy neutrino ($\sim10^{22}$ eV) in the relic neutrino background (the so-called Z-burst model) [9] is another possible scenario which is a hybrid of astrophysical zevatrons with new particles [10].

In general, top-down and hybrid scenarios predict a rather high flux of UHE neutrinos exceeding the observed cosmic ray flux. Gamma rays account for a part or most of the highest energy cosmic rays above 10^{20} eV, whereas nucleons would dominate at lower energies. Thus the primary composition, especially the gamma ray content (referred to as the gamma/proton ratio), is a powerful discriminator between the models of UHE cosmic ray origin. It should be mentioned that even within conventional bottom-up models one can expect a significant gamma/proton ratio due to the decay of neutral pions produced in cosmic ray interactions with the 2.7 K CMB photons. Under certain circumstances (extragalactic magnetic field strength, distance to the sources, maximal proton energy, slope of the proton energy spectrum, etc.), the subsequent electromagnetic cascade in the intergalactic space can lead to an UHE gamma ray flux comparable to the observed cosmic ray flux [11,12].

Air showers initiated by UHE gamma rays have characteristic features in comparison with ''ordinary'' hadronic showers. Two effects must be taken into account for a study of air shower development in the case of gamma ray primaries—the *Landau-Pomeranchuk-Migdal* (LPM) effect and *cascading in the geomagnetic field*.

The influence of the LPM effect [13,14] on shower development has been studied by many authors during the last 30

years. The effect reduces the Bethe-Heitler (BH) cross sections for bremsstrahlung and pair production at energies $\gtrsim 10^{19}$ eV in the atmosphere, leading to a significant elongation of the electromagnetic shower and large fluctuations in the shower development. Generally, this effect is well understood although there is no commonly accepted standard code taking into account the LPM effect in electromagnetic shower modeling. It should be pointed out that other possible mechanisms of suppression of bremsstrahlung and pair creation processes at extremely high energies have to be more carefully studied [15].

Once the electron-positron pair is produced in UHE gamma ray interaction with the geomagnetic field away from the Earth's surface, it initiates an electromagnetic ''cascade'' due to synchrotron radiation before entering the atmosphere. As a result, the energy of the primary gamma ray is shared by a bunch of lower energy secondary particles which are mainly photons and a few electron-positron pairs. The influence of the LPM effect on subsequent showers in the atmosphere is significantly weakened.

The history of electromagnetic cascade calculations in the geomagnetic field is also quite long since it started with the work of McBreen and Lambert [16]. The main results of previous works [12,17–20] are in good agreement. Recent calculations refined the previous ones, revealing some practically important features in the cascading process. For example, in [21] it is shown that the study of two major components of the giant air showers, the size spectra and muon content, can reveal the nature of the UHE cosmic rays if the specific dependence on the shower arrival direction is observed. Some observables that can be extracted from the Pierre Auger Observatory detectors (longitudinal profiles, lateral distribution, and front curvature) are discussed in [22]. In [23] the technique of adjoint cascade equations was applied to study UHE gamma ray shower characteristics in the geomagnetic field and in the atmosphere, emphasizing the muon component of air shower.

The aim of the present paper is to study in detail the UHE gamma ray shower characteristics that are measurable by air fluorescence detectors. It is also important to know the difference in longitudinal shower development between gamma ray and hadronic showers, which can be used for an effective separation between these primary species. In the following, we will discuss the dependence of UHE gamma ray shower characteristics on the incident direction and the possibility of detecting such showers in future experiments.

II. ELECTROMAGNETIC INTERACTIONS IN A MAGNETIC FIELD

About 60 years ago soon after Auger's discovery of extensive air showers, Pomeranchuk [24] estimated the maximal energy of primary cosmic ray electrons and gamma rays that is allowed to enter the atmosphere after interactions with the geomagnetic field. According to his calculations, the maximal electron energy E_c due to radiation in the geomagnetic field is a few times 10^{17} eV ($\sim 4\times 10^{17}$ eV for electrons vertically incident on the geomagnetic equatorial plane). Whatever energy greater than E_c the electrons have, they lose it rapidly down to below E_c. The analogous gamma ray energy due to pair creation in the geomagnetic field is $\sim 6\times 10^{19}$ eV.

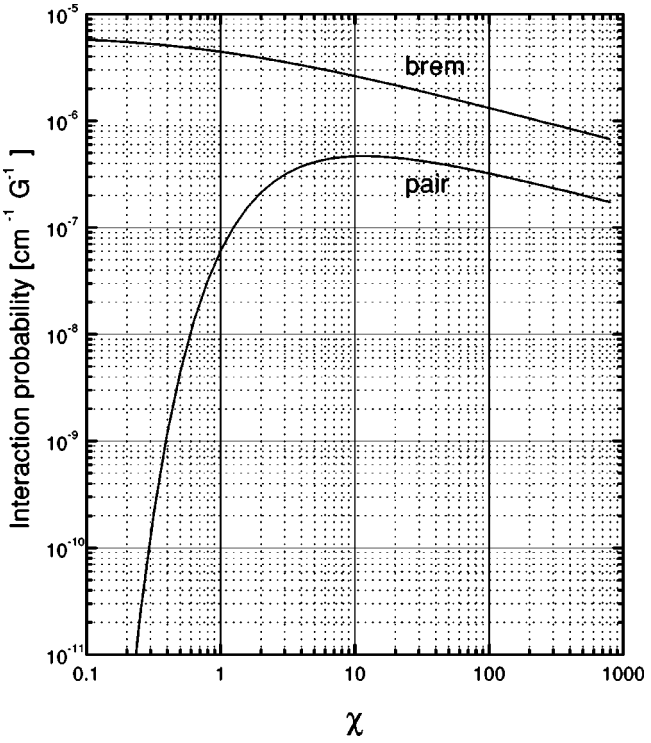

FIG. 1. The total probabilities (cross sections) for magnetic bremsstrahlung and pair production as a function of parameter χ.

Similar to cascading in matter, the main elementary processes leading to particle multiplication in a magnetic field are magnetic bremsstrahlung (synchrotron radiation) and magnetic pair production. It is well known that essentially nonzero probabilities for magnetic bremsstrahlung and pair production require both strong field and high energies [25]. The relevant parameter determining the criteria for this is

$$\chi = \frac{E}{mc^2}\frac{H_\perp}{H_{\rm cr}} \tag{1}$$

where E is the particle energy, $H_\perp$ is the magnetic field strength (the component perpendicular to the particle trajectory), m is the electron mass, and $H_{\rm cr}=4.41\times 10^{13}$ G.

The total probabilities (cross sections) for radiation and pair production for a given value of the magnetic field strength depend only on χ and are shown in Fig. 1. Magnetic pair production has significant probability for $\chi \geqslant 0.1$. For effective shower development, however, one needs even higher values of $\chi \geqslant 1$ because the radiated photon spectrum becomes harder with increasing χ. The maximal photon energy estimated by Pomeranchuk ($\sim 6\times 10^{19}$ eV) comes from the condition $\chi \sim 1$.

We use the expressions of Bayer *et al.* [26] for the differential probabilities (per unit length) for magnetic bremsstrahlung and magnetic pair production:

$$\pi(\varepsilon,\omega)d\omega=\frac{\alpha m^2}{\pi\sqrt{3}}\frac{d\omega}{\varepsilon^2}\left[\left(\frac{\varepsilon-\omega}{\varepsilon}+\frac{\varepsilon}{\varepsilon-\omega}\right)K_{2/3}\left(\frac{2u}{3\chi}\right)-\int_{2u/3\chi}^{\infty}K_{1/3}(y)dy\right] \quad (2)$$

for bremsstrahlung, and

$$\gamma(\omega,\varepsilon)d\varepsilon=\frac{\alpha m^2}{\pi\sqrt{3}}\frac{d\varepsilon}{\omega^2}\left[\left(\frac{\omega-\varepsilon}{\varepsilon}+\frac{\varepsilon}{\omega-\varepsilon}\right)K_{2/3}\left(\frac{2u_1}{3\chi}\right)+\int_{2u_1/3\chi}^{\infty}K_{1/3}(y)dy\right] \quad (3)$$

for pair creation, where ε and ω are the electron and photon energies and $u=\omega/(\varepsilon-\omega)$, $u_1=\omega^2/\varepsilon(\omega-\varepsilon)$. Here $\hbar=c=1$. $K_\nu(z)=\int_0^\infty e^{-z\cosh(t)}\cosh(\nu t)dt$ is the modified Bessel function known as MacDonald's function.

While for $\chi\gg 1$ (strong field) the electromagnetic cascade develops similarly to a cascade in matter [27], in the case of $\chi\leqslant 1$ the photon interaction length increases sharply with decreasing photon energy. Electrons continue to radiate and the shower becomes a bunch of secondary photons carrying more than 94–95 % of the primary energy.

III. SIMULATION

In our simulation studies of air showers initiated by gamma rays and hadrons (proton or iron), we use the AIRES code (version 2.2.1) [28] incorporated in the QGSJET hadronic interaction model [29]. AIRES includes the LPM effect in simulation of electromagnetic showers. For simulations of electromagnetic cascades in the geomagnetic field we use our original code.

To simulate showers initiated by UHE gamma rays, we first model cascading in the geomagnetic field starting with a single UHE gamma ray far away from the Earth's surface down to the top of the atmosphere. Then secondary particles that reach the top of atmosphere are set as an input for the AIRES code. Finally, the air shower initiated by the UHE gamma ray is constructed as a superposition of lower energy gamma ray subshowers. In practice, we use a library of presimulated showers in the atmosphere that has been calculated by the AIRES code.

A. Electromagnetic cascading in a geomagnetic field

We simulate the electromagnetic cascade in the geomagnetic field by injecting a UHE gamma ray at a distance of $3R_e$ away from the Earth's surface where R_e is the Earth's radius of 6.38×10^8 cm. The primary gamma ray and secondary particles are propagated by taking account of pair production and synchrotron radiation at each step (a step size of 1 km). Only particles above a threshold energy of 10^{16} eV are followed in the simulation until they reach the top of the atmosphere. This threshold energy is low enough to neglect the contribution of subthreshold particles in the cascade.

In order to examine the properties of electromagnetic cascades as a function of the incident direction, we uniformly divide the sky into bins of 5 ° for both azimuth and zenith angles giving 1085 points and simulate 50 events for each point. In our simulation we use the International Geomagnetic Reference Field (IGRF) and world magnetic model which provide a good approximation for the geomagnetic field up to 600 km above sea level [30]. Above this altitude the geomagnetic field is extrapolated from this model.

In the present work we examine the properties of UHE gamma ray showers for the location in Utah (longitude $=113.0\,°$ W, latitude$=39.5\,°$ N, and 1500 m above sea level) near the site of the HiRes experiment. In this location, the IGRF gives a field of 0.53 G pointing 25 ° downward from 14 ° east of the geographical (true) north.

B. Atmospheric shower simulation

The simulations of atmospheric showers were carried out independently of the geomagnetic cascading process. Using the AIRES code, we first prepared a library of subshowers initiated by gamma rays with zenith angles of 39.7 °, 54 °, and 61.6 ° and energy fixed between 10^{16} and 10^{21} eV at logarithmically equally spaced values (ten energies per decade). The number of all charged particles was recorded at 5 g cm^{-2} intervals in vertical depth. The library contains 500 showers at each energy. It should be noted that this number is significantly greater than the maximal number ($\sim$100) of secondary gamma rays from the geomagnetic cascade in each energy bin.

The construction of an UHE gamma ray initiated shower is carried out by a method similar to the so-called bootstrap method as follows. The ith secondary particle with energy $E_i^{(\mathrm{GM})}$ at the top of the atmosphere is followed by a subshower with the nearest energy $E_i^{(\mathrm{atm})}$ selected randomly from the library. The secondary electron is replaced by a gamma ray with the same energy. By summing up the subshowers $(i=1,\ldots,N_\gamma^{(\mathrm{GM})})$ with a weight $w_i=E_i^{(\mathrm{GM})}/E_i^{(\mathrm{atm})}$, the atmospheric shower initiated by a single gamma ray with energy $E_0^{(\gamma)}$ is represented as a superposition of subshowers with total energy $\Sigma^{N\gamma}w_iE_i^{(\mathrm{atm})}=E_0^{(\gamma)}$.

In the present work we also simulated samples of 500 hadron (proton and iron) initiated showers for the same zenith angles and energy range to compare the results.

IV. RESULTS

A. Properties of geomagnetic cascading

The cascade development is determined by the features of the cross sections of the processes and the field strength. The maximal values of the parameter χ which governs cascading do not much exceed 1, e.g., $\chi=1.33$ for 10^{20} eV and $H_\perp=0.3$ G, and $\chi=13.3$ for 10^{21} eV and the same $H_\perp$, i.e., one can expect only a few gamma ray interactions (pair creations) in the shower. But such $H_\perp$ values are characteristic for the surface of the Earth. The field strength rapidly decreases with the geocentric distance, $\sim 1/R_e$, which means that the cascade starts not far from the surface of the Earth. The first interaction of the gamma rays with the energies of

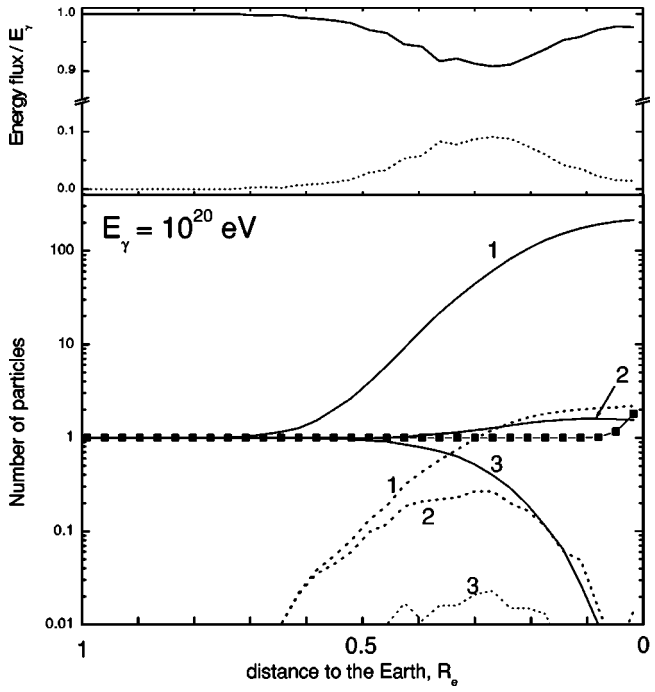

FIG. 2. Shower profile (bottom panel) in the geomagnetif field for primary gamma ray with energy 10^{20} eV and different threshold energies: $1-10^{16}$ eV, $2-10^{19}$ eV, and $3-5\times10^{19}$ eV. The zenith angle is 40 ° and the azimuth corresponds to the north. Solid and dotted curves indicate for photons and electrons, respectively. Curves with symbols show the number of photons with energies $>10^{16}$ eV in showers with the same primary energy and azimuth from the south. The energy flux carried by photons (solid curve) and electrons (dotted curve) is shown on the top panel for azimuth from the north. R_e is the Earth's radius ($=6.38\times10^8$cm).

interest occurs in relatively narrow range of distances not further than $3R_e$. For example, the mean altitude of the first interaction of vertical gamma rays with primary energy $E_0^{(\gamma)}=10^{21}$ eV is about 5300 km.

The typical shower profiles averaged over 1000 showers for $E_0^{(\gamma)}=10^{20}$ eV and different threshold energies for secondary photons and electrons are shown in Fig. 2 (bottom panel). The zenith angle is 40 ° and the azimuth corresponds to north (strong field). For comparison in this figure is also shown the shower profile for the secondary photons with energy above 10^{16} eV in a shower coming from the south (weak field). This picture differs too much from the cascade development in matter. As the primary energy is distributed between the electron and photon components (see the top panel of Fig. 2), the mean photon energy decreases, and when $\chi<1$ the mean free path for pair production sharply increases (see Fig. 1). The energy of the electron component starts to return quickly to the photon component and the shower converts to a beam of photons carrying the bulk of the primary energy. For the case shown in Fig. 2 (strong field) the mean number of gamma ray interactions per shower in the geomagnetic field is approximately 1 (1.11 for the sample of 1000 showers) which means that there is almost no pair creation after the initial interaction. For $E_0^{(\gamma)}=5\times10^{20}$ eV and the same conditions this number increases to 4.16. This is the reason for the much smaller number of electrons than photons in the shower. In our example, for the strong field, the mean number of electrons reaching the top of the atmosphere, is 2.22 ($=2\times1.11$) for 10^{16} eV threshold energy. These electrons carry $\sim2\%$ of the primary energy. In the case of weak field (line with symbols in Fig. 2), the probability of the primary gamma ray to interact in the geomagnetic field is only $\sim6-7$ % and this happens on an average of 200 km from the sea level.

In Utah, the southern sky region is close to the direction of the geomagnetic field and hence the effect of geomagnetic cascading is relatively small. Gamma rays arriving from the northern sky region travel through stronger field whose strength increases with the zenith angle. Generally, primary gamma rays are most affected by the geomagnetic field when they come from the northern sky or near the horizon.

Figure 3 shows maps for the gamma ray conversion (interaction) probability (gray scale) with the geomagnetic field for all incident directions in horizontal coordinates. The different panels correspond to primary energies $E_0^{(\gamma)}=10^{19.5}$, 10^{20}, $10^{20.5}$, and 10^{21} eV. The radial coordinate is the zenith angle θ. The inner circles correspond to $\theta=30$ ° and 60 °, and the outer one is of the horizon. Azimuths are as labeled.

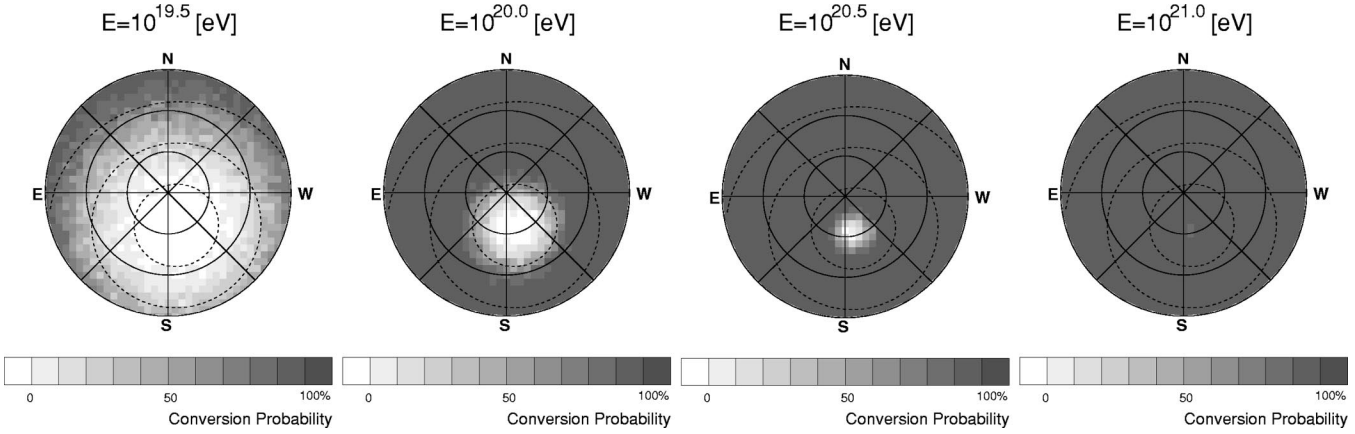

FIG. 3. Maps of gamma ray conversion probability in the geomagnetic field for primary energies $10^{19.5}$, 10^{20}, $10^{20.5}$, and 10^{21} eV. Inner circles correspond to zenith angles 30 °, 60 °, and horizon.

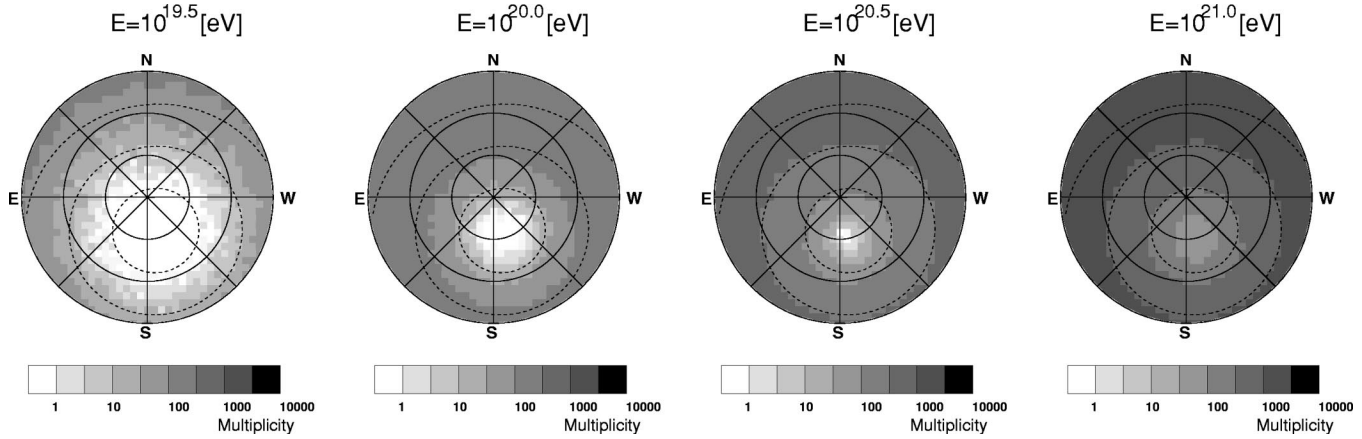

FIG. 4. Maps of average multiplicity of secondary particles with energy $>10^{16}$ eV at the top of the atmosphere. Primary gamma ray energies and coordinates are the same as in Fig. 3.

''N'' denotes the true north). Dashed curves indicate opening angles of 30°, 60°, and 90° to the local magnetic field.

The region with smaller probability is around the direction that is parallel to the local geomagnetic field. From this region, primary gamma rays are most likely to enter the atmosphere without interaction. Thus, this region can be referred to as the ''window'' for the primary gamma rays. Through this window they can reach the top of the atmosphere surviving interaction and be observed as LPM showers. The size of this window shrinks rapidly with increasing primary energy and almost all gamma rays with $E_0^{(\gamma)} \gtrsim 10^{20}$ eV initiate a geomagnetic cascade above the atmosphere.

Figure 4 shows maps of the average multiplicity of the secondary particles (number of electrons plus photons above 10^{16} eV; gray scale) at the top of the atmosphere on the same coordinates as in Fig. 3. The average energy of secondary particles ($E_0^{(\gamma)}$/multiplicity) is plotted in Fig. 5.

The patterns of these maps match the field strength well, i.e., the direction of the geomagnetic field at the ground level, which reflects the fact that the first interaction occurs not far from the Earth's surface.

For low primary energy and/or weak field strength, i.e., small $E_0^{(\gamma)} H_\perp$, the primary gamma ray does not or only once produces an electron pair before reaching the top of the atmosphere. The electrons produced continuously radiate photons by magnetic bremsstrahlung and the multiplicity increases with the primary energy. Nevertheless, radiated photons can hardly interact again with the geomagnetic field unless $\chi \gtrsim 1$.

For the direction with very strong field (or very high primary energy), i.e., large $E_0^{(\gamma)} H_\perp$, e.g., for the northern sky region or near-horizontally incident gamma rays, the multiplicity is almost proportional to the primary energy which leads to a nearly constant average particle energy at the top of the atmosphere (see Fig. 5). This energy is about a few times of 10^{17} eV. In the sky regions where the conversion probability is 100% the maximal average energy of the secondary particles, which are mainly photons, do not exceed several times 10^{19} eV. This is consistent with the estimation by Pomeranchuk [24] described previously and thus the LPM effect is ineffective in the atmosphere except for the window regions.

The multiplicity distributions of secondary particles at the top of the atmosphere for different incident zenith angles (39.7°, 54°, and 61.6°) and azimuths corresponding to north and south are plotted in Fig. 6. Each histogram includes 1000 simulated showers.

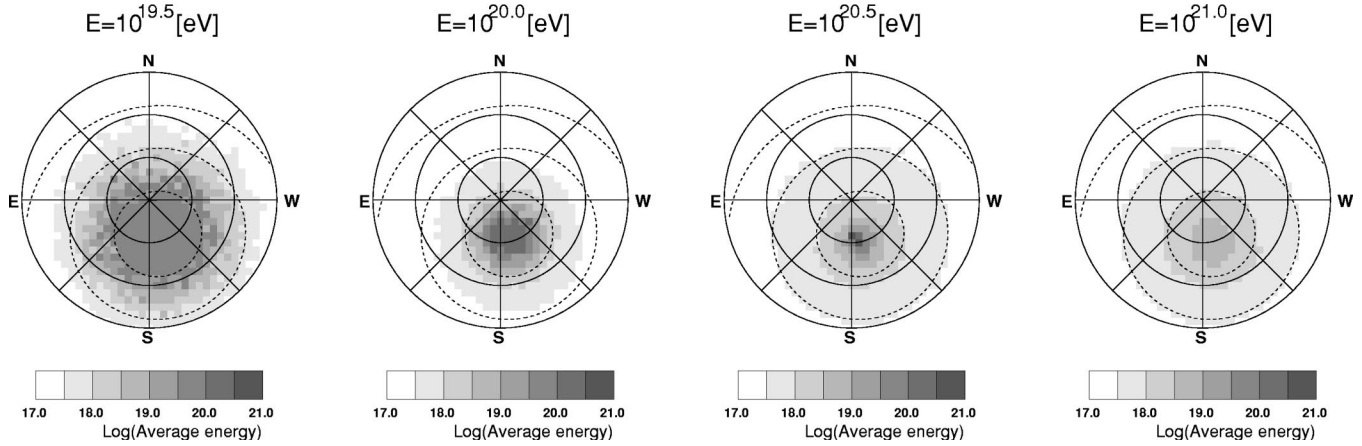

FIG. 5. Maps of average energy of secondary particles with energy $>10^{16}$ eV at the top of atmosphere. Primary gamma ray energies and coordinates are the same as in Figs. 3 and 4.

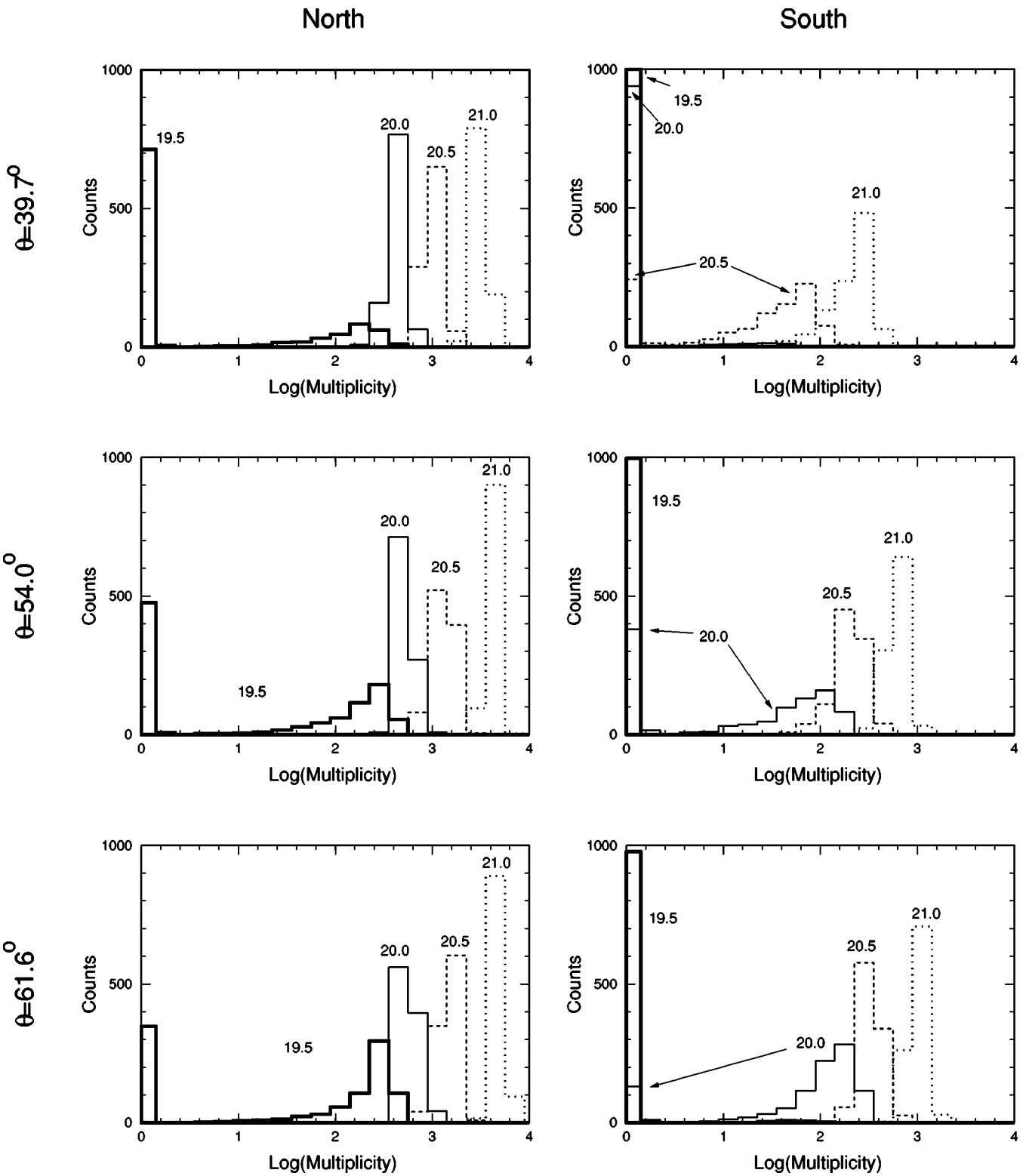

FIG. 6. Multiplicity distribution of secondary particles (photons plus electrons) at the top of the atmosphere for primary energies of $10^{19.5}$, 10^{20}, $10^{20.5}$, and 10^{21} eV and different zenith angles of 39.7°, 54°, and 61.6°. Arrival directions of gamma rays are from north and south.

The columns in the first bin of each panel correspond to the primary gamma rays that do not interact in the geomagnetic field. In regions with 100% conversion probability the fluctuations are small for large $E_0^{(\gamma)}H_\perp$ due to the better cascade development by more gamma ray interactions above the atmosphere.

Figure 7 shows the average energy distribution (spectrum) of secondary particles at the top of the atmosphere. The data

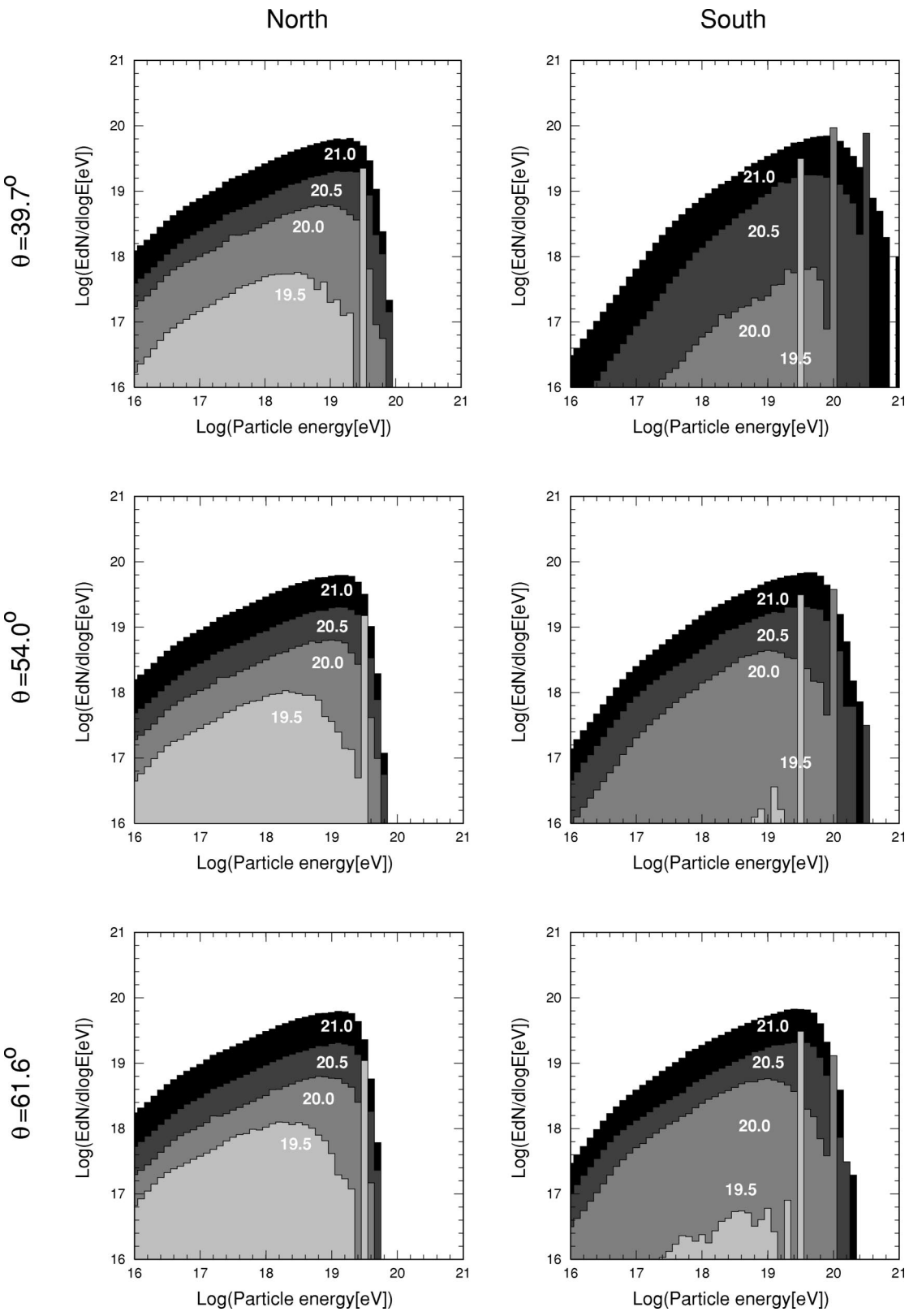

FIG. 7. Energy distribution (spectrum) of secondary particles (photons plus electrons) at the top of the atmosphere. Each panel corresponds to that in Fig. 6.

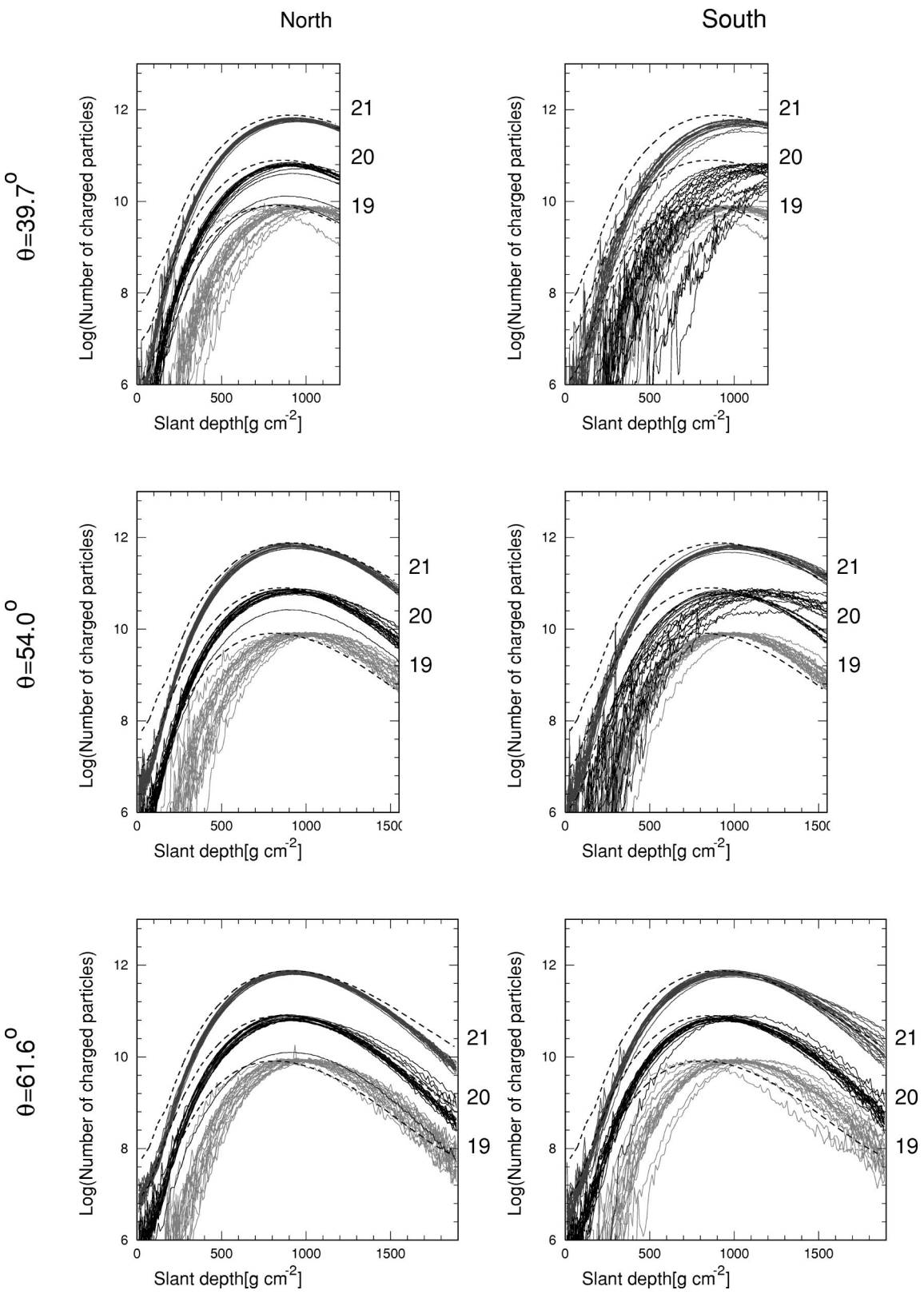

FIG. 8. Longitudinal development of individual gamma ray showers in the atmosphere for primary energies of 10^{21}, 10^{20}, and 10^{19} eV (from top) and different zenith angles of 39.7°, 54°, and 61.6°. Arrival azimuths are from the true north and south. Dashed curves correspond to average shower developments for proton primaries calculated with QGSJET model.

belong to the same set of simulated showers as in Fig. 6. Here the ''surviving'' primary gamma rays manifest themselves by the columns in the last bins of some histograms.

The maximum of the spectrum shifts toward the higher energies when $E_0^{(\gamma)}$ increases. However, except for the cases where the probability of survival primaries is large, i.e., the conversion probability is not close to 100%, this shift slows down for $E_0^{(\gamma)} > 10^{20}$ eV and the shape of the spectrum remains almost the same for the highest energies. As mentioned previously, the multiplicity of secondaries is almost proportional to $E_0^{(\gamma)}$. The spectra display sharp cutoffs at a few times 10^{19} eV and subsequent subshowers in the atmosphere are not affected by the LPM effect. We discuss this in the next subsection.

We estimate the lateral spread of particles at the top of the atmosphere. All particles are contained within a radius of about 10 cm. This value is much greater than 0.1 mm given in [16,19] but is still too small to be taken into account. Thus, successive shower developments in the atmosphere can be correctly expressed as a superposition of atmospheric subshowers initiated by secondary particles with such energy spectra.

B. Shower development in the atmosphere

Figure 8 shows examples of individual shower development initiated by primary gamma rays with $E_0^{(\gamma)} = 10^{19}$, 10^{20}, and 10^{21} eV. Left and right panels correspond to azimuths from north and south, respectively. Zenith angles are 39.7°, 54°, and 61.6°. Dashed curves represent the average shower profiles for proton primaries.

This figure illusrates very well a remarkable feature of the shower development at these energies—significantly small fluctuations in the case that the primary gamma ray interacts with the geomagnetic field. The largest fluctuations in the shower development can be found for $E_0^{(\gamma)} = 10^{20}$ eV, $\theta = 39.7°$, and incident direction from the south. In this case the primary gamma ray conversion probability in the geomagnetic field is only several percent and the LPM effect strongly affects the shower development in the atmosphere. Increasing primary energy leads to a significant decrease of fluctuations and this trend is stronger for the sky regions close to the horizon (large $H_\perp$). These two effects are more pronounced for northern sky regions.

Figure 9 shows distributions of the depth of the shower maximum in the atmosphere $X_{\max}$ for showers with $E_0^{(\gamma)} = 10^{19}$, $10^{19.5}$, 10^{20}, $10^{20.5}$, and 10^{21} eV. We present the cases of zenith angles of 54° and 61.6° in the left and right panels, respectively. In each panel, the solid line indicates the distribution of proton showers. Dotted and dashed lines represent those for gamma ray showers from the azimuths of north and south, respectively.

The shape of $X_{\max}$ distributions of gamma ray showers noticeably varies with primary energy and incident direction. As the primary energy increases, the distributions become narrower and the mean values are almost constant for energies $> 10^{20}$ eV (see also Fig. 11 below). Some distributions having two maxima or a long tail to deeper $X_{\max}$ result from

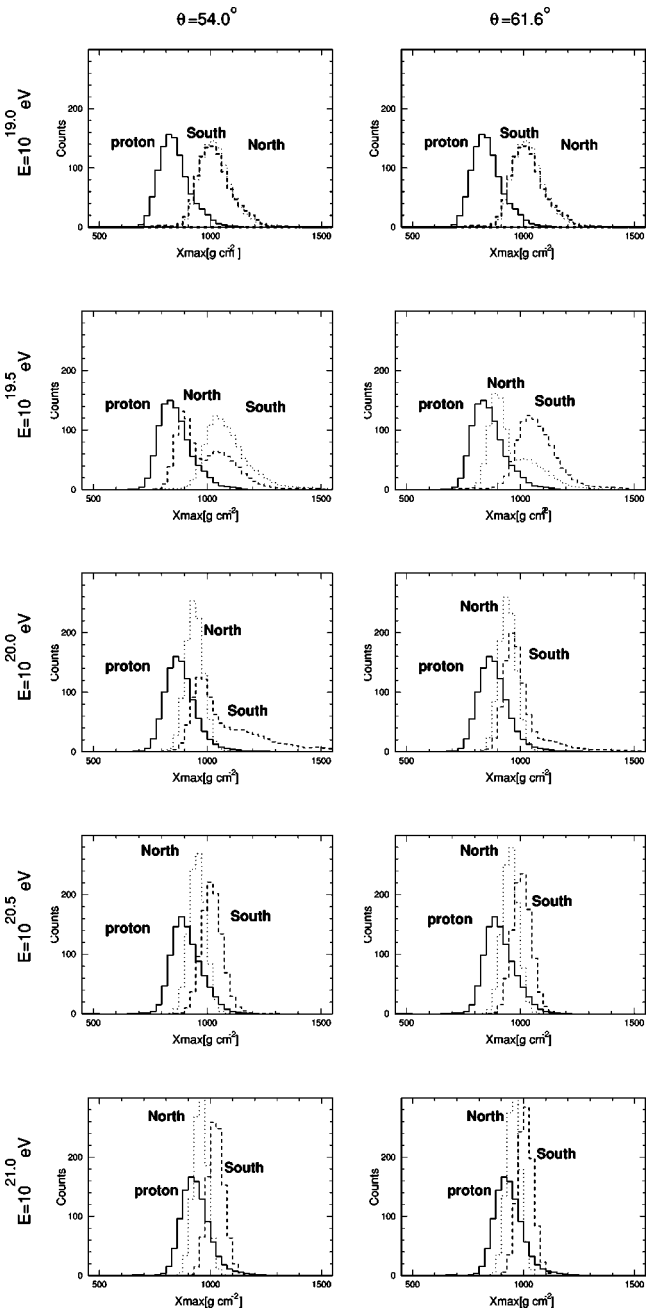

FIG. 9. $X_{\max}$ distributions for proton and gamma ray showers for primary energies of 10^{19}, $10^{19.5}$, 10^{20}, $10^{20.5}$, and 10^{21} eV and different zenith angles of 54° and 61.6°. Azimuths are north (dotted lines) and south (dashed lines).

a mixture of converted and not converted gamma rays above the atmosphere.

In Fig. 10, maps of average $X_{\max}$ are shown on the same coordinates as in Figs. 3–5.

The data for this figure are obtained by the following approximation. The simulation of the shower development is based on the method described in the previous section. For a given zenith angle we use data from the library of presimulated showers with similar zenith angle. Since the magnitude of the LPM effect depends on the atmospheric density profile along the particle trajectory, there is a small dependence on

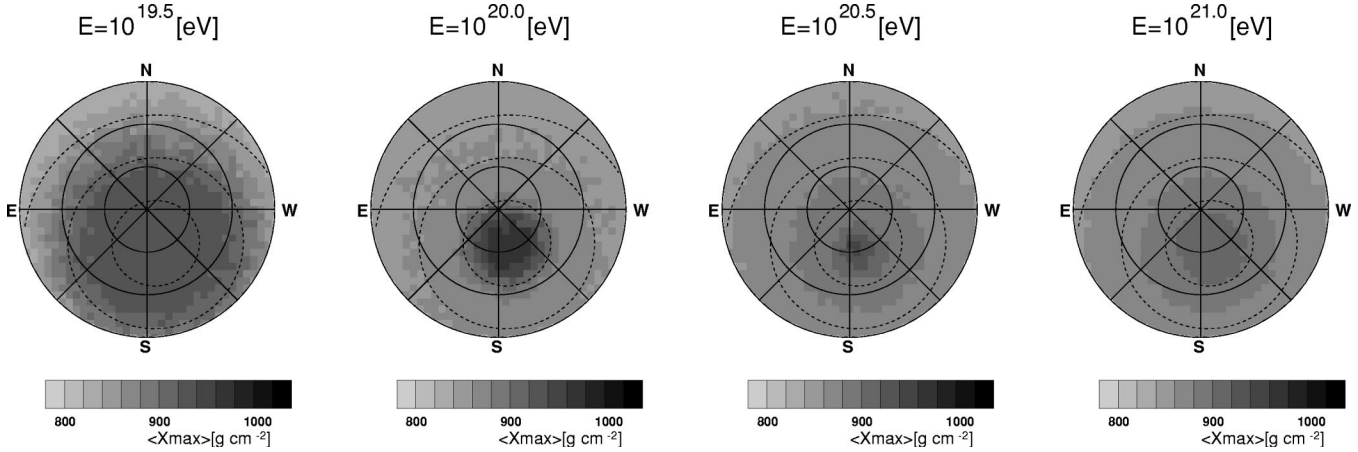

FIG. 10. Maps of average depth of shower maximum $\langle X_{\max} \rangle$ in the atmosphere for primary energies $10^{19.5}$, 10^{20}, $10^{20.5}$, and 10^{21} eV. Coordinates are the same as in Fig. 4.

the incident zenith angle. In the vertical region for 10^{20} eV, this effect possibly matters and $\langle X_{\max} \rangle$ can be higher than shown due to the lack of an air shower library for this direction. For higher primary energy or other sky region, however, primary gamma rays are converted and thus it is not necessary to take into account the LPM effect for the estimation of $\langle X_{\max} \rangle$.

In each map, i.e., for each $E_0^{(\gamma)}$, $\langle X_{\max} \rangle$ reflects the dependence of geomagnetic cascading on the incident direction. Typically, gamma ray showers with larger $\langle X_{\max} \rangle$ are predominantly coming from the southern sky region. Only for 10^{20} eV is there a small window where gamma ray showers are affected by the LPM effect. This region may serve as a probe for UHE gamma ray presence.

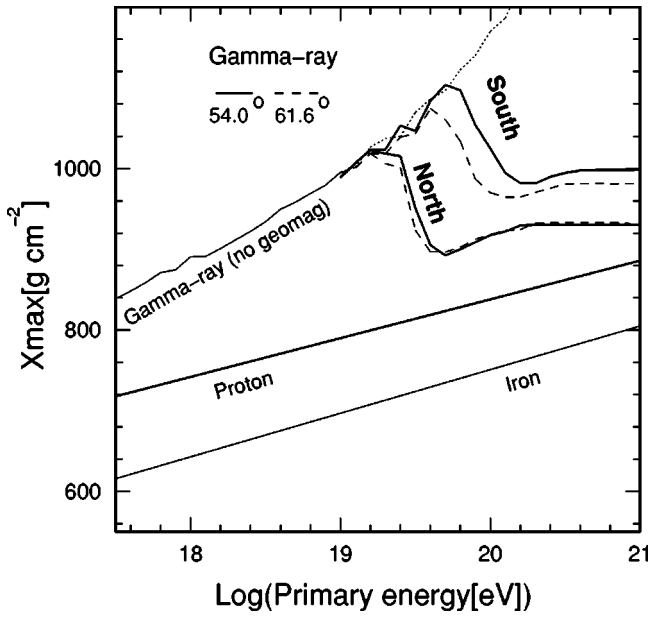

FIG. 11. The average depth of shower maximum $\langle X_{\max} \rangle$ in the atmosphere as a function of primary energy for gamma ray showers. Corresponding relations for proton and iron are also drawn by solid lines. Arrival directions of gamma rays are from north and south as denoted. The dotted curve indicates the case of no geomagnetic field. Dashed line and thick solid curves are for zenith angles of 54° and 61.6°, respectively.

Figure 11 shows the relation between $\langle X_{\max} \rangle$ and $E_0^{(\gamma)}$ for gamma ray showers. For comparison, corresponding relations for proton and iron primaries are also drawn in the figure. The incident azimuths of the gamma rays are from north and south. The dashed lines and thick solid lines are for zenith angles of 54° and 61.6°, respectively. The dotted curve indicates the case of no geomagnetic field.

For proton and iron showers $\langle X_{\max} \rangle$ increases with $E_0^{(\gamma)}$ and the slopes of the relations, i.e., the elongation rates, are almost constant and are 54 and 56 g cm^{-2}/decade, respectively. The elongation rate for gamma ray showers is greater than those of hadronic ones and is also constant according to the electromagnetic cascade theory up to energies $\sim 2 \times 10^{19}$ eV. Above this energy the LPM effect steepens the relation of $\langle X_{\max} \rangle$ versus $E_0^{(\gamma)}$ as shown by the dotted line in the figure.

Geomagnetic cascading starts to ''work'' approximately at the same energy, about several times 10^{19} eV. At this energy, which depends on the incident direction, $\langle X_{\max} \rangle$ reaches its maximum. Above this energy the geomagnetic cascade develops well enough to suppress the LPM effect in the atmosphere. This leads to a rapid decrease of $\langle X_{\max} \rangle$.

The slow increase of $\langle X_{\max} \rangle$ after its minimum results from the slow increase of the fraction of secondary photons above the threshold for the LPM effect (see Fig. 7). The multiplicity also increases proportionally to $E_0^{(\gamma)}$ which leads to almost constant average photon energy in the bunch above 10^{20} eV. It must be noted that a superposition of BH subshowers has smaller $\langle X_{\max} \rangle$ than a single BH shower with an energy equal to the sum of the subshower energies.

In Fig. 12, the fluctuations of $X_{\max}$ (the standard deviation of the $X_{\max}$ distribution) are shown as a function of primary energy. The line key is the same as in Fig. 11 but the case of no geomagnetic field is not shown.

Similar to $\langle X_{\max} \rangle$, the fluctuations for gamma ray showers vary typically depending on primary energy and incident direction, while those for proton and iron showers are almost constant, ~ 67 g cm^{-2} and ~ 26 g cm^{-2}, respectively.

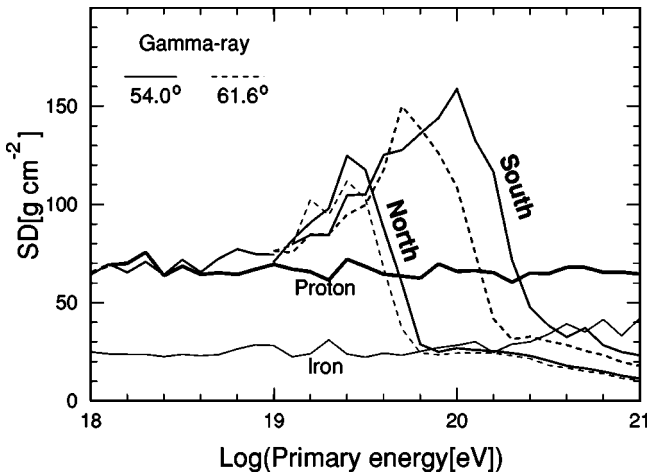

FIG. 12. Fluctuations (standard deviation σ) of $X_{\max}$ as a function of primary energy. The line key is as in Fig. 11 but the case of no geomagnetic field is not shown.

For gamma ray showers, the picture between 19^{19} and 10^{20} eV is similar to that in Fig. 11. Large fluctuations are due to the LPM effect. For energies at which the geomagnetic cascading is effective, the fluctuations decrease rapidly with increasing energy. At the highest energies, the fluctuations tend to be as small as those for iron showers. This behavior is attributed to a competition between the LPM effect and geomagnetic cascading as in Fig. 11.

V. DISCUSSION AND CONCLUSIONS

Our study shows that the longitudinal development of gamma ray showers is not simply scaled with primary energy. Shower development in the energy region above $\sim 10^{19.5}$ eV shows very specific dependence on both the primary energy and incident direction. The $\langle X_{\max} \rangle$ of gamma ray showers is larger than that expected for proton showers. Furthermore, the elongation rate of gamma ray showers shows considerable variation with energy depending on their incident directions. The future observation of these longitudinal shower characteristics with better statistical accuracy would be the possible key for studying the UHE gamma ray flux. Also, additional information may be obtained from the properties of $X_{\max}$ fluctuations.

In order to acquire definite conclusions on the primary composition of UHE cosmic rays, more elaborate considerations may be required due to limited statistics and difficulty in separating gamma ray and hadronic showers. For example, as is shown above, the fluctuations of $X_{\max}$ for gamma ray showers become even smaller than those for proton showers and are close to those for iron showers above 10^{20} eV. We expect that the development of a number of UHE showers will be measured with better accuracy in the near future, which will be the first decisive step in looking for UHE gamma rays.

If the observed showers develop slowly from the sky region near the window (see Figs. 2–4 and 9) showing typical characteristics of LPM showers, this could be a noticeable and physically important evidence of UHE gamma ray presence.

As was earlier mentioned in [21], the magnetic bremsstrahlung process may be important for shower development at high altitudes where the atmospheric density is very low. According to the estimations in [31], made by numerical integration of the system of cascade equations, the interaction of shower particles with the geomagnetic field inside the atmosphere becomes important for cascades created by primary gamma rays with energies higher than $\sim 3 \times 10^{20}$ eV. For example, injecting gamma rays with energy 10^{20} eV vertically into the atmosphere, the number of particles in showers at sea level calculated only with the LPM effect is $\sim 13\%$ less than that in showers when interactions with the geomagnetic effect (for $H_{\perp} = 0.35$ G) are taken into account. This difference increases with increasing primary energy up to ~ 2.5 times for 10^{21} eV. Using our own simple hybrid code for one-dimensional atmospheric shower simulation we obtain similar results, showing also a noticeable shift of the shower maximum. This work is now in progress.

Planned projects (Auger [32], EUSO [33], etc.) to study UHE cosmic rays promise to observe individual shower development with better accuracy. It is important to find effective and reasonable physical parameters from simulation studies in order to discriminate gamma ray showers from hadronic ones on an event by event basis. It can also be a strong probe by including a fluctuation study in addition to average shower development in discussions about the composition of UHE cosmic rays.

ACKNOWLEDGMENTS

We thank T. Stanev for valuable help and discussions. H.P.V. is thankful to the Japan Society for the Promotion of Science (JSPS) for support of his visit to Japan where this work was conceived, and to the National Graduate Institute for Policy Study (GRIPS) for its hospitality.

[1] M. Nagano and A. A. Watson, Rev. Mod. Phys. **72**, 689 (2000).
[2] H. Ohoka *et al.*, Nucl. Instrum. Methods Phys. Res. A **385**, 268 (1997).
[3] C. C. H. Jui *et al.*, in *Proceedings of the 27th International Cosmic Ray Conference*, Hamburg, Germany (Copernicus Gesellshaft, Kaltenburg-Lindau, 2001), Vol. 1, p. 354.
[4] B.N. Afanasiev *et al.*, in *Proceedings of the Tokyo Workshop on Techniques for the Study of the Extremely High Energy Cosmic Rays*, Tanashi, Tokyo, 1993, edited by M. Nagano (Institute of Cosmic Ray Research, University of Tokyo), p. 32.
[5] K. Greisen, Phys. Rev. Lett. **16**, 748 (1966); G. T. Zatsepin and V. A. Kuz'min, Pis'ma Zh. Éksp. Teor. Fiz. **4,** 114 (1966) [JETP Lett. **4**, 78 (1966)].
[6] P. Bhattachrjee and G. Sigl, Phys. Rep. **327**, 109 (2000), and references therein.
[7] P. Bhattacharjee, C. T. Hill, and D. N. Schramm, Phys. Rev.

Lett. **69**, 567 (1992).
[8] V. Berezinsky, P. Blasi, and A. Vilenkin, Phys. Rev. D **58**, 103515 (1998).
[9] T. J. Weiler, Phys. Rev. Lett. **49**, 234 (1982).
[10] A. Olinto, Nucl. Phys. B (Proc. Suppl.) **110**, 434 (2002).
[11] F. Halzen, R. Protheroe, T. Stanev, and H. Vankov, Phys. Rev. D **41**, 342 (1990); J. Wdowczyk and A. W. Wolfendale, Astrophys. J. **349**, 35 (1990).
[12] F. A. Aharonian, B. L. Kanewsky, and V. V. Vardanian, Astrophys. Space Sci. **167**, 111 (1990).
[13] L. D. Landau and I. J. Pomeranchuk, Dokl. Akad. Nauk SSSR **92**, 535 (1953) (in Russian).
[14] A. B. Migdal, Phys. Rev. **103**, 1811 (1956).
[15] S. Klein, Rev. Mod. Phys. **71**, 1501 (1997).
[16] B. McBreen and C. J. Lambert, Phys. Rev. D **24**, 2536 (1981).
[17] H. P. Vankov and P. Stavrev, Phys. Lett. B **266**, 178 (1991).
[18] S. Karakula and W. Bednarek, in *Proceedings of the 24th International Cosmic Ray Conference*, Rome, Italy (INFN, Rome, 1995), Vol. 1, p. 266.
[19] K. Kasahara, in *Proceedings of International Symposium on EHECR: Astrophysics and Future Observations*, Tokyo, Japan, 1996, edited by M. Nagano (Institute for Cosmic Ray Research, University of Tokyo, 1997), p. 221.
[20] W. Bednarek, astro-ph/9911266; astro-ph/011061.
[21] T. Stanev and H. P. Vankov, Phys. Rev. D **55**, 1365 (1997).
[22] X. Bertou, P. Billoir, and S. Dagoret-Campagne, Astropart. Phys. **14**, 121 (2000).
[23] A. V. Plyasheshnikov and F. A. Aharonian, J. Phys. G **238**, 267 (2002).
[24] I. Pomeranchuk, Pis'ma Zh. Éksp. Teor. Fiz. **9**, 915 (1939) (in Russian).
[25] T. Erber, Rev. Mod. Phys. **38**, 626 (1966).
[26] V. H. Bayer, B. M. Katkov, and V. S. Fadin, *Radiation of Relativistic Electrons* (Atomizdat, Moscow, 1973) (in Russian).
[27] V. Anguelov and H. Vankov, J. Phys. G **25**, 1755 (1999).
[28] S. J. Sciutto, astro-ph/9911331.
[29] N. N. Kalmykov and S. S. Ostapchenko, Phys. At. Nucl. **56**, 346 (1993).
[30] Distributed by National Geophysical Center, Boulder, Colorado, http://www.ngdc.noaa.gov
[31] B. L. Kanevsky and A. I. Goncharov, Vopr. At. Nauki Tekh., Ser.: Tekh. Fiz. Eksp. **4**, 34 (1989); A. I. Goncharov, Thesis, Tomsk Polytechnical Institute, 1991 (in Russian).
[32] AUGER Collaboration website: www.auger.org
[33] EUSO Collaboration website: www.ifcai.pa.cnr.it/~EUSO/